Chalcogenide Letters Vol. 15, No.6, June 2018, p. 345 - 351

PHOTOCATALYTIC AND THERMOELECTRIC PROPERTIES OF WURTZITE Cu_2NiSnS_4 NANOCRYSTALS VIA SOLVOTHERMAL METHOD

H. GUAN*, X. GU, X. CHEN
School of Materials Science and Engineering, Yancheng Institute of Technology, 9 Yinbing Street, Yancheng 224051, PR China

Wurtzite Cu_2NiSnS_4(CNTS) nanocrystals were successfully synthesized by the solvothermal method. X-ray diffraction (XRD), Raman spectroscopy and scanning electron microscopy (SEM) show that pure CNTS exhibit sheet-like structure being composed of small nanocrystals with size of about 10-20nm and idea band gap(~1.41eV). Ethylenediamine(en) plays an important role in the wurtzite phase formation. The degradation rate of methylene blue(MB) with under visible-light irradiation is about 85.1%. The Seebeck coefficient(S) and electrical conductivity(σ) can reach to 57.82$\mu V \cdot K^{-1}$ and 12.48$S \cdot m^{-1}$ at 675*K*. It indicates that CNTS can be useful for effective visible-light photocatalyst and high-temperature thermoelectric material.

(Received April 12, 2018; Accepted June 9, 2018)

Keywords: Semiconductors, Cu_2NiSnS_4, Nanocrystals, Solvothermal, Photocatalytic, Thermoelectric

1. Introduction

In recent decades, the semiconductor powders such as $CuInSe_2$, $Cu_2InGa(Se,S)_4$, CdTe, Bi_2Te_3, etc. have attracted considerable attention owing to their application in the fields of photovatic, photocatalysis and thermoelectric[1-5]. However, the rarity of indium(In) and tellurium(Te) and the toxicity of cadmium(Cd) limits their usage. Therefore, searching for earth-abundant, inexpensive and environment friendly chalcogenide materials has become one of the hot spots. As a novel energy conversion material, Cu_2ZnSnS_4 (CZTS) containing abundant and non-toxic elements has received great interest for application in the fields of photovatic, photocatalysis and thermoelectric [6-9]. We believe that Cu_2NiSnS_4(CNTS) is also considered as possible energy conversion material due to its analogous structure to CZTS. Several methods such as solvothermal, hot injection, electrospinning and spray were utilized to synthesize CNTS compounds [10-17]. Among the solution-based chemical methods, the solvothermal method has advantages in controlling size and elemental composition of nanoparticles. To date, there is only a report on the synthesis of wurtzite CNTS nanocrystals via a solvothermal method, and the research focused on the superparamagnetic behavior and optical property [18]. However, to the best of our knowledge, there have been no reports on the photocatalytic and thermoelectric properties of wurtzite CNTS nanocrystals via solvothermal method.

*Corresponding author: guanhao1980@sina.com

In this paper, we synthesized wurtzite CNTS nanocrystals by a solvothermal method, and investigated their structure, morphology, photocatalytic and thermoelectric properties.

2. Experimental details

$CuCl_2 \cdot 2H_2O$(Analytical Reagent), $Ni(CH_3COO)_2 \cdot 4H_2O$(Analytical Reagent), $SnCl_2 \cdot 2H_2O$ (Analytical Reagent) and H_2NCSNH_2(Analytical Reagent) were used without further purification. In a typical experiment, $CuCl_2 \cdot 2H_2O$ (0.025M), $Ni(CH_3COO)_2 \cdot 4H_2O$ (0.0125M), $SnCl_2 \cdot 2H_2O$ (0.0125M) and H_2NCSNH_2 (0.05M) were added in 80ml ethylenediamine to dissolve under magnetic stirring. The autocave was sealed and maintained at 200℃ for 12h. Then the autocave was naturally cooled down to room temperature. The products were washed several times with deionized water and dried in vacuum at 80℃ for 3h.

In a photocatalystic experiment, 0.05g of CNTS was added to 50ml of MB solution with the concerntration of 10^{-5}mol/l. Then the solutions were stirred in the dark for 30min ensure the balance of adsorption and desorption of MB before the ones exposed to visible light irradiation under sustained stirring. At given time intervals, 5ml of the as-obtained solution were used as measured samples after removing CNTS nanocrystals by centrifugation. In a thermoelectric experiment, the CNTS nanocrystals were utilized to prepare a pellet sample by hot-pressing sintering.

The crystal structure was characterized using a PANalytical X'Pert PRO diffractometer with Cu$K\alpha$ radiation (λ=0.15406nm) and JY-T64000 Raman spectrometers. The microstructure was investigated using LEO-1530VP scanning electron microscope. The photocatalytic property was measured using Shimadzu UV2450 spectrophotometer. The thermoelectric properties were measured using Namicro-Ⅲ thermoelectric parameters measurement.

3. Results and discussion

The typical XRD pattern of as-obtained CNTS nanocrystals is shown in Fig.1(a). The major XRD diffraction peaks appeared at 2θ=27.2°, 28.5°, 31.2°, 47.6°, 51.8° and 56.2° corresponding to (100), (002), (101), (110), (103) and (112) planes of wurtzite CNTS, respectively. This result matches well with the literature values[18]. No other characteristic peaks of secondary phases are detected, indicating pure wurtzite CNTS phase was obtained. According to the Debye-Scherrer formula, the average crystallite size of CNTS nanocrystals can be calculated to be about 15.5nm. The formation of wurtzite CNTS is attributed to the usage of ethylenediamine(en) in our work. The strong coordination between ethylenediamine(en) and metal cations can reduce the surface energy to form metastable wurtzite crystal structure. The formation process can be explained as follows: First, the cations of metal salt reacted with en to form the $[M(en)_2]^{n+}$ complex. Second, the rapid formation (nucleation) of $Cu_{2-x}S$ occured. At last, Sn and Ni replaced parts of Cu to form wurtzite CNTS structure.

Although XRD identified the phase, which should be further distinguished due to the similarity of XRD patterns of CNTS and mesophase Cu_2SnS_3. So the structure of wurtzite CNTS nanocrystals was further investigated by Raman spectrum at room temperature. It can be seen from Fig.1(b) that only a strong peak at 333cm^{-1} corresponding to CNTS was observed, which is nearly

related to the value of stannite CNTS nanocrystals in literature [12]. The Raman peaks corresponding to Cu_2SnS_3 (267cm^{-1}, 303cm^{-1} and 352cm^{-1}) were excluded. The result mentioned above is in good agreement with XRD analysis.

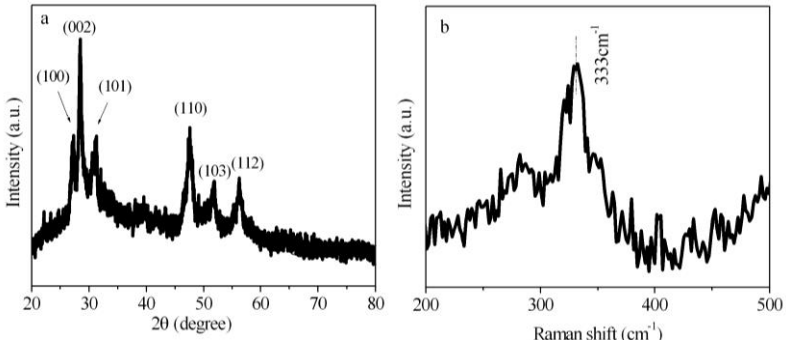

Fig. 1. XRD pattern(a) and Raman spectrum(b) of CNTS nanocrystals.

The morphologies of as-obtained CNTS nanocrystals are shown in Fig. 2. It can be seen that CNTS nanocrystals are composed of irregular sheet-like particles. From high magnification in Fig. 2(b), we can observe that the particles are formed by agglomeration of small nanocrystals with size of about 10-20 nm, which is in accordance with the value obtained by XRD analysis above. The CNTS sheet-like particles are formed through oriented aggregation of CNTS nanocrystals [19-21]. The sheet-like structure can increase their surface areas significantly, which are benifit for the photocatalytic activity.

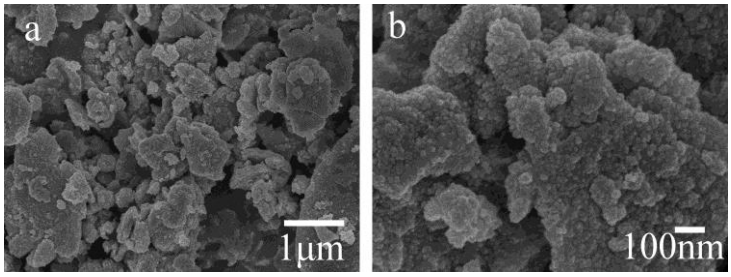

Fig. 2. Low(a) and high magnification(b) SEM images of CNTS nanocrystals.

As we all know, the optical characteristic is a crucial property of photocatalyst. The optical bandgap energy of the CNTS nanocrystals can be estimated from the $(\alpha hv)^2$ against hv graph (α=absorbance, h=Planck's constant and v=frequency) by extrapolating the linear absorption edge part of the curve. It can be seen from Fig. 3 that the optical bandgap of the CNTS nanocrystals is around 1.41eV, indicating suitable optical properties for visible light photocatalytic.

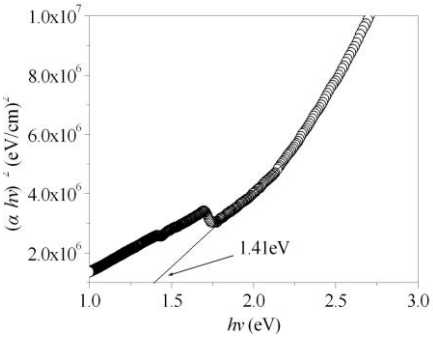

Fig. 3. Optical bandgap estimations of CNTS nanocrystals.

In order to evaluate of the photocatalytic property of CNTS nanocrystals, we examine the decomposition of methylene blue(MB) under visible-light irradiation for different time, in which MB is chosen as a typical organic waste model. Fig. 4 shows the temporal evolution of the spectra during the photogradation of MB. From Fig. 4(a), we can see that the strength of the absorption peak is reduced with the increasing of the exposure time, indicating that CNTS nanocrystals have excellent visible light photocatalytic decomposition of MB. To investigate the degradation rate, the photocatalytic degradation rates(C/C_0) of the MB with and without CNTS nanocrystals are shown in Fig. 4(b). After 100min of visible-light irradiation, MB without CNTS decomposes only about 3%, indicating that self-degradation of MB could be neglected. While that with the addition of CNTS decomposes about 85.1%. The results show that CNTS is an excellent applicant of visible-light photocatalyst. The stability of wurtzite CNTS is investigated by recycling the photocatalyst for degradation of MB under visible-light irradiation. As shown in Fig.4(c), there is no apparent deactivation of the photocatalyst after reuse 3 times, indicating the good stability of wurtzite CNTS nanocrystals.

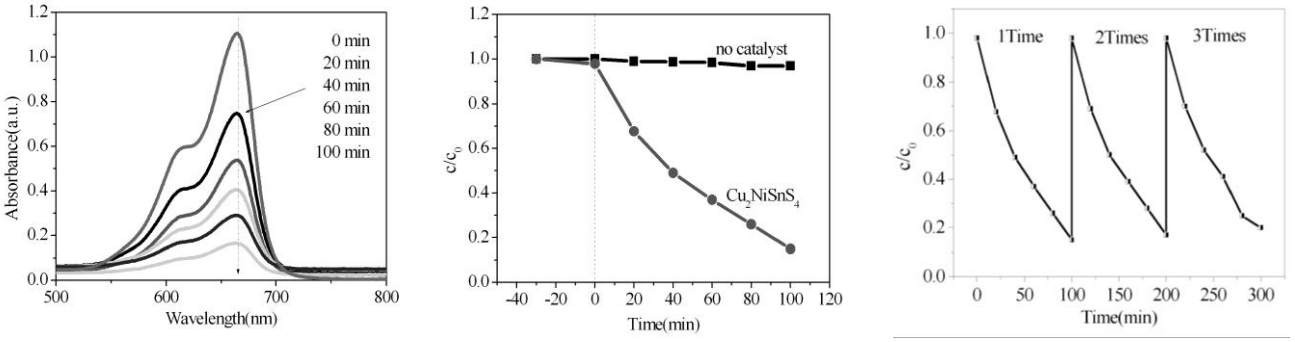

Fig. 4. (a) Time-dependent absorption spectra of a solution of MB in the presence of the CNTS nanocrystals under visible light irradiation (b)the photodegradation rate of MB as a function of different time with and without the addition of CNTS nanocrystals (c) The photo stability of CNTS nanocrystals.

A possible schematic mechanism is shown in Fig. 5. The as-synthesized *p*-type CNTS semiconductor nanocrystals have holes as main carriers for the oxidation resistance, which can result in the redox reactions with adsorbed species over the surface of CNTS catalysts. when Uv-Vis irradiation exposed over a catalyst, generation of h^+-e^- take place. Then these charge

carriers migrate on the surface of CNTS catalyst, where a redox reaction takes place with other species which presents on the CNTS catalyst surface. h^+ reacts with H_2O or OH^- easily to produce •OH. In addition, e^- reacts with O_2 to produce $\bullet O_2^-$, and •OH can be obtained further. The produced •OH can oxidize degradation the contaminant. The specific photocatalytic process as follows:

$$CNTS + h\nu \rightarrow CNTS + h^+ + e^- \quad (1)$$

$$h^+ + OH^- \rightarrow \bullet OH \quad (2)$$

$$h^+ + H_2O \rightarrow \bullet OH + H^+ \quad (3)$$

$$e^- + O_2 \rightarrow \bullet O_2^- \quad (4)$$

$$\bullet O_2^- + H^+ \rightarrow \bullet OOH \quad (5)$$

$$2 \bullet OOH \rightarrow H_2O_2 + O_2 \quad (6)$$

$$H_2O_2 + e^- \rightarrow \bullet OH + OH^- \quad (7)$$

$$MB + \bullet OH \rightarrow \text{degradation products} \quad (8)$$

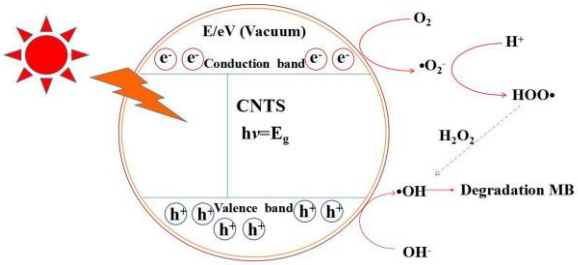

Fig. 5. Illustration of photocatalytic redox reaction occurring via photocatalysis to produce •OH to react with MB dye.

CNTS have the potential to be a thermoelectric material due to its low thermal conductivity. The curves of temperature dependent Seebeck coefficient(*S*) and electrical conductivity(σ) are shown in Fig.6. We can see that CNTS exhibits *P*-type nature owing to the positive value of Seebeck coefficient(*S*). The Seebeck coefficient(*S*) and electrical conductivity(σ) increase with the temperature increasing. The Seebeck coefficient(*S*) changed from 28.37μV•K^{-1} to 57.82μV•K^{-1} over a temperature range of 325-675*K*. The large Seebeck coefficient(S) is caused by contribution of spin entropy of magnetic ions Ni^{2+}.The electrical conductivity(σ) changed from 3.45S•m^{-1} to 12.48S•m^{-1} over a temperature range of 325-675*K*. The high electrical conductivity(σ) is closely related to narrow band-gap.

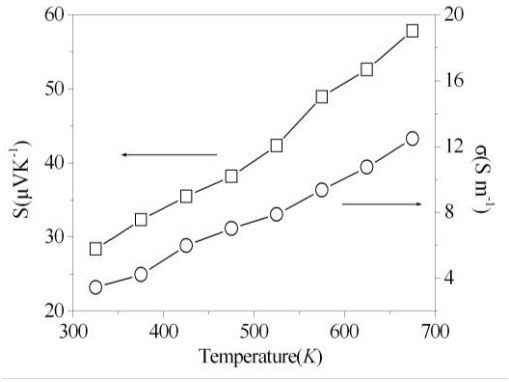

Fig. 6. Temperature-dependent plot of Seebeck coefficient and electrical conductivity of CNTS sample.

4. Conclusions

In summary, wurtzite CNTS were synthesized via the solvothermal method. The prepared CNTS is composed of sheet-like nanoparticles. The possible formation process of CNTS was discussed. The as-synthesized CNTS nanocrystals could degrade about 85.1% of the methylene blue(MB) within 100min under visible-light irradiation, indicating a potential candidate for visible-light photocatalyst to treating pollutants in waste water. The large Seebeck coefficient(S) and high electrical conductivity(σ) are obtained. The novel thermoelectric properties of bulk CNTS can be for high-temperature thermoelectric devices.

Acknowledgement

This research is financial supported by Top-notch Academic Programs Project of Jiangsu Higher Education Institutions (PPZY2015A025).

References

[1] M. Bär, I. Repins, M. A. Contreras, L. Weinhardt, R. Noufi, C. Heske, Appl. Phys. Lett. **95**, 052106 (2009).
[2] M. G. Kanatzidis, Chem. Mater. **22**, 648 (2010).
[3] V. A. Akhavan, M. G. Panthani, B. W. Goodfellow, D. K. Reid, B. A. Korgel, Opt. Express **18**, A411 (2010).
[4] Q. Guo, G. M. Ford, H. W. Hillhouse, R. Agrawal, Nano. Lett. **9**, 3060 (2009).
[5] M. Bagheri, A. R. Mahjoub, B. Mehri, RSC Adv. **4**, 21757 (2014).
[6] C. Steinhagen, M. G. Panthani, V. Akhavan, B. Goodfellow, B. Koo, B. A. Korgel, J. Am. Chem. Soc. **131**, 12554 (2009).
[7] J. Xu, X. Yang, Q. D. Yang, T. L. Wong, C. S. Lee, J. Phys. Chem. C **116**, 19718 (2012).
[8] H. R. Yang, L. A. Jauregui, G. Q. Zhang, Y. P. Chen, Y. Wu, Nano. Lett. **12**, 540 (2012).
[9] X. Hou, Y. Li, J. Yan, C. Wang, Mater. Res. Bull. **60**, 628 (2014).

[10] T. Wang, Y. Li, H.i Liu, H. Li, S. Chen, Mater. Lett. **124**, 148 (2014).
[11] A. Kamble, K. Mokurala, A. Gupta, S. Mallick, P. Bhargava, Mater. Lett. **137**, 440 (2014).
[12] S. Sarkar, B. Das, P. R. Midya, G. C. Das, K. K. Chattopadhyay, Mater. Lett. **152**, 155 (2015).
[13] G. Sahaya Dennish Babu, X. Sahaya Shajan, S. Alwin,V. Ramasubbu, G. M. Balerao, J. Electron. Mater. **47**, 312 (2018).
[14] S. Yuan, S. Wang, L. Li, Y. Zhu, X. Zhang, J. Yan, ACS Appl. Mater. Interfaces **8**, 9178 (2016).
[15] F. Ozel, E. Aslan, B. Istanbullu, O. Akay, I. H. Patir, Appl. Catal. B: Environ. **198**, 67 (2016).
[16] F. Ozel. J. Alloy. Compd. **657**, 157 (2016).
[17] N. Bitri, S. Dridi, F. Chaabouni, M. Abaab, Mater. Lett. **213**, 31 (2018).
[18] Y. Cui, R. Deng, G. Wang, D. Pan, J. Mater. Chem. **22**, 23136 (2012).
[19] S. Bahramzadeh, H. Abdizadeh, M. R. Golobostanfard, J. Alloy. Compd. **642**, 124 (2015).
[20] Y. Zhou, W. Zhou, M. Li, Y. Du, S. Wu, J. Phys. Chem. C **115**, 19632 (2011).
[21] F. Chen, J. Zai, M. Xu, X. F. Qian, J. Mater. Chem. A **1**, 4316 (2013).